Int. J. Heat Mass Transfer. Vol. 34, No. 3, pp. 843–852, 1991
Printed in Great Britain

0017–9310/91 $3.00 + 0.00

Numerical simulation of convection in the two-phase zone of a binary alloy

QIUPING YU and YAOHE ZHOU
Department of Materials Science and Engineering, Northwestern Polytechnical University, Xi'an 710072, China

(*Received* 6 *December* 1989)

Abstract—The main equations for the numerical simulation of convection in a two-phase zone based on a model of the continuum approach to a porous medium are advanced. In order to solve non-linear computation caused by the interaction of unknown variables in the equations, the trial-and-error method is used. The size and extent of interdendritic flow at different times are indicated from calculated velocity profiles. It is shown that the radial back-flow area due to natural convection corresponds to the mushy zone above the 625°C isotherm under conditions of a small cooling rate. With increasing the cooling rate, the flow due to the siphonic force becomes more and more important.

1. INTRODUCTION

INTERDENDRITIC fluid flow in a two-phase zone is a very important transport phenomenon during solidification, and gives rise to some defects in an alloy. The driving forces causing the fluid flow include siphonic force due to solidification shrinkage (or expansion) and gravity acting on a fluid of variable density, etc. Mehrabian *et al.* [1] pointed out that with changing cooling conditions there may be three modes of interdendritic flow, i.e. stable flow, intermediate flow, and unstable flow. The natural convection of the mushy zone due to gravity leads to unstable flow which can cause some casting defects such as channel segregation, etc.

In general, a mushy zone during solidification is described with a model of a porous medium. The mushy zone, however, has its own features different from the porous medium, such as (1) latent heat of solidification, (2) variable liquid fraction (or void fraction), and (3) solute distribution at liquid–solid interface, etc. It is necessary that the energy, mass, and momentum transport equations for the porous medium be corrected with the features mentioned above.

A numerical computation method has often been adopted in engineering problems to perform quantitative analysis of liquid convection in the mushy zone in recent years. Ridder *et al.* [2] gave an analysis of the effect of fluid flow in axisymmetric ingots of continuous casting and electroslag remelting. Maples and Poirier [3] analysed the transients of convection in the two-phase zone for unidirectional and horizontal solidification. Bennon and Incropera [4] applied a continuum model to investigate the solidification of aqueous ammonium chloride solution in the presence of an imposed forced flow. However, numerical simulation of convection in the mushy zone is still under development. This is because (1) the mechanism of the convection must be described with several physical equations which interact with each other, and it is difficult to combine them in calculation; (2) the mathematical models of some single-valued conditions for the equations are also being probed.

An axisymmetric unsteady-state model of convection in the mushy zone has been computed in this paper. What is called unsteady-state here is only that $\nabla T/\varepsilon$ is not constant during solidification. Al–4.5Cu alloy ingots freeze under different solidifying conditions, as shown in Table 1 [5].

2. ANALYSIS

2.1. *Fundamental equations*

The main equations for numerical simulation of convection in a two-phase zone have been advanced on the basis of a model of the continuum approach to a porous medium. Essential to the treatment of two-phase fluids as continua is the concept of a particle [6]. One advantage of adopting the model is that various equations, describing conservation of energy, mass, and momentum, etc. in continua, can be applied to the two-phase zone. A set of equations can be expressed as follows for the system discussed in this paper [7].

2.1.1. *Energy equation.*

$$\left(1-\beta f_{\mathrm{L}}+\frac{H_{\mathrm{f}}}{c_p}\frac{\partial f_{\mathrm{L}}}{\partial T}\right)\frac{\partial T}{\partial t}=\frac{1}{c_p\bar{\rho}}\nabla\cdot(\lambda\nabla T)$$
$$-(1-\beta)f_{\mathrm{L}}\mathbf{V}\cdot\nabla T \quad (1)$$

where $(H_{\mathrm{f}}/c_p)(\partial f_{\mathrm{L}}/\partial T)$ refers to the latent heat of solidification, and the second term on the right-hand side of equation (1) refers to the effect of interdendritic flow on energy transport.

2.1.2. *Mass conservation equation.*

$$\frac{\partial\bar{\rho}}{\partial t}=-\nabla\cdot\rho_{\mathrm{L}}f_{\mathrm{L}}\mathbf{V} \quad (2)$$

where

NOMENCLATURE

c_p specific heat
C_L liquid concentration
$\bar{C}_s$ average solid concentration
f_L, f_s volume fraction of liquid and solid, respectively
$\mathbf{g}$ acceleration due to gravity
h heat transfer coefficient
H_f latent heat of solidification
$H(r)$ height of liquid metal pool, a function of r
k equilibrium partition ratio
K permeability
$\mathbf{n}$ unit vector normal to isotherm
N buoyancy ratio
P pressure
P_a pressure at top of metal pool
P_L pressure acting on liquidus
Q velocity ratio, equation (25)
r radial coordinate
R radius of ingot
t time
T temperature
T_A ambient temperature
T_B boundary temperature
T_p freezing point of pure aluminium
$\mathbf{U}$ velocity of isotherm
$\mathbf{U}_E$ velocity of eutectic isotherm
U_{rE}, U_{zE} component of $\mathbf{U}$ in the r- and z-direction, respectively
$\mathbf{V}$ interdendritic flow velocity
V_c flow velocity due to convection
$\mathbf{V}_P$ component of $\mathbf{V}$ in the $\mathbf{n}$-direction
$\mathbf{V}_s$ flow velocity due to siphonic force
V_{rP}, V_{zP} component of $\mathbf{V}_P$ in the r- and z-direction, respectively
z axial coordinate.

Greek symbols
β solidification shrinkage, $(\rho_s-\rho_L)/\rho_s$
β_c concentration coefficient of volume expansion
β_T temperature coefficient of volume expansion
ν constant for equation (11), etc.
ε cooling rate
λ thermal conductivity
μ dynamic viscosity
ρ density
$\bar{\rho}$ average density, $\rho_L f_L+\rho_s f_s$
ρ_L liquid density in two-phase zone
ρ_s solid density
ρ_{L0} datum liquid density of alloy
ρ_{sE}, ρ_{LE} density of eutectic–solid and eutectic–liquid, respectively.

$$\frac{\partial\bar{\rho}}{\partial t}=\frac{\partial}{\partial t}(\rho_L f_L+\rho_s f_s). \tag{3}$$

In addition, the solute conservation equation should be considered for a binary alloy system

$$\frac{\partial(\bar{\rho}\bar{C})}{\partial t}=-\nabla\cdot\rho_L f_L C_L\mathbf{V} \tag{4}$$

where

$$\frac{\partial(\bar{\rho}\bar{C})}{\partial t}=\frac{\partial}{\partial t}(\bar{C}_s\rho_s f_s+C_L\rho_L f_L). \tag{5}$$

After essential assumptions are given [8], combining equation (4) with equation (2) provides a local solute redistribution in the mushy zone during solidification

$$\frac{1}{f_L}\frac{\partial f_L}{\partial t}=-\frac{1-\beta}{1-k}\left(1+\frac{\mathbf{V}\cdot\nabla T}{\varepsilon}\right)\frac{1}{C_L}\frac{\partial C_L}{\partial t}. \tag{6}$$

The assumptions for deriving equation (6) are as follows. (1) A small volume element in the mushy zone is large enough that the solid fraction within it at any time is exactly the local average, but small enough that it can be treated as a differential element. (2) There is no movement of the solid phase into or out of the element. (3) Solute enters or leaves the element only by liquid flow to feed shrinkage. (4) Mass flow in or out of the element by diffusion is neglected. (5) Solidification occurs with equilibrium at the solid–liquid interface so that there is no undercooling, and the rate of solidification is controlled only by the rate of heat transfer and convection within the mushy zone. (6) The local temperature and the composition of the solid at the interface are specified by the local composition of the liquid. (7) Diffusion in the solid is negligible. (8) Solid density is constant. (9) No pore forms during solidification.

2.1.3. *Velocity equation.* Darcy's law for flow through a porous medium is useful for describing the interdendritic flow in the mushy zone, thus

$$\mathbf{V}=-\frac{K}{\mu f_L}(\nabla P+\rho_L\mathbf{g}). \tag{7}$$

2.1.4. *Pressure equation.* In equation (7), the interdendritic flow velocity is linearly related to the pressure gradient. Combining equations (3), (6), and (7) with equation (2) (see Appendix) provides an expression for the pressure distribution in the mushy zone

$$\frac{\partial^2 P}{\partial r^2}+\frac{\partial^2 P}{\partial z^2}+A_P\frac{\partial P}{\partial r}+B_P\frac{\partial P}{\partial z}+C_P=0 \tag{8}$$

where

$$A_P = \frac{1}{r} + \frac{2}{f_L}\frac{\partial f_L}{\partial r} + \frac{b_1}{\rho_L}\frac{\partial T}{\partial r}$$

$$B_P = \frac{2}{f_L}\frac{\partial f_L}{\partial z} + \frac{b_1}{\rho_L}\frac{\partial T}{\partial z}$$

$$C_P = g\frac{\partial \rho_L}{\partial z} + \frac{2g\rho_L}{f_L}\frac{\partial f_L}{\partial z} + b_1 g\frac{\partial T}{\partial z} - b_1\frac{\mu f_L}{K\rho_L}\frac{\partial T}{\partial t}$$

$$b_1 = \frac{dC_L}{dT}\left(\frac{\partial \rho_L}{\partial C_L} - \frac{\rho_L(\rho_L - \rho_s)}{\rho_s(1-k)C_L}\right).$$

2.2. *Effect of liquid density*

Variance of a fluid density due to temperature and concentration differences can cause a buoyancy force which forms natural convection in the fluid. In addition, a siphonic force is also related to the density in the light of the meaning of solidification shrinkage. The close relation between convection and liquid density is directly reflected in the above equations, in which the liquid density of the mushy zone ρ_L exists. ρ_L is a function of temperature T and liquid concentration C_L, i.e. $\rho_L = \rho_L(T, C_L)$, and from the binary phase diagram the concentration is also a function of temperature, thus

$$\frac{d\rho_L}{dT} = \left(\frac{\partial \rho_L}{\partial T}\right)_{C_L} + \left(\frac{\partial \rho_L}{\partial C_L}\right)_T \frac{dC_L}{dT}. \quad (9)$$

The dependence of the liquid density on temperature can be derived from equation (9)

$$\rho_L = \rho_{L0} - \left(\frac{\partial \rho_L}{\partial C_L}\right)_T \frac{dC_L}{dT}(T_P - T) - \left(\frac{\partial \rho_L}{\partial T}\right)_{C_L}(T_P - T). \quad (10)$$

The density variance due to concentration difference is generally greater than that due to temperature difference during solidification, i.e. $(\partial\rho_L/\partial C_L)_T > (\partial\rho_L/\partial T)_{C_L}$ in equation (9). dC_L/dT is always less than zero for an alloy of $k < 1$. $d\rho_L/dT < 0$ if $(\partial\rho_L/\partial C_L)_T > 0$ and $d\rho_L/dT > 0$ if $(\partial\rho_L/\partial C_L)_T < 0$ from equation (9). Two different patterns of natural convection in a two-phase zone, as shown in Fig. 1, are formed due to the positive or negative value of $d\rho_L/dT$. It will be seen below that Al–4.5Cu alloy is an alloy of $d\rho_L/dT < 0$ and the convection pattern similar to Fig. 1(a) is caused in its ingot.

2.3. *Model of permeability*

The permeability K, which can determine the magnitude of interdendritic flow velocity, is a very important parameter in the two-phase zone. K is also a variable since f_L always varies during solidification. In the early investigation [1]

$$K = vf_L^2. \quad (11)$$

After the permeability of interdendritic space is measured using a translucent material having the same casting structure as metallic alloys, Murakami *et al.* give the following form [9]:

$$K \propto d_L f_L^3 \quad (12)$$

where d_L is the primary dendrite-arm spacing. Having taken some patterns deriving Darcy's law into consideration, we generally adopt the equation

$$K = vf_L^n \quad (13)$$

where $n \geqslant 2$, which depends on the casting structure during solidification.

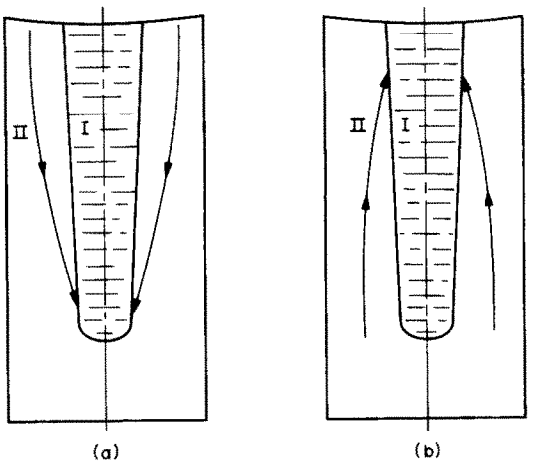

FIG. 1. Two patterns of natural convection in the mushy zone: (a) $d\rho_L/dT < 0$; (b) $d\rho_L/dT > 0$.

3. NUMERICAL METHOD

A finite difference method of the differential equation is used here [10]. A rectangular area sectioned through the axis of the ingot symmetry is divided by the square network and $\Delta r = \Delta z = 2$ mm.

3.1. *Trial-and-error method*

Temperature T is the dependence on f_L and V in equation (1) and in turn f_L is on it in equation (6). Such cases also exist in other equations. These interactions make the simulation computation hard to solve. In former works the temperature distributions are supposed beforehand to simplify the computation [3, 11]. In order that the numerical simulation of the convection in the mushy zone can approach the practice process in an ingot as much as possible, computation in this paper is based on a set of equations including energy equation (1). The computation procedure is shown with a flow chart in Fig. 2 after specifying essential single-valued conditions for the equations, the model provides: (1) temperature field, (2) density distribution, (3) pressure field, (4) velocity field, (5) liquid fraction distribution, and (6) concentration field, etc.

The interaction with each other, due to control of an unknown variable in an equation by variables in

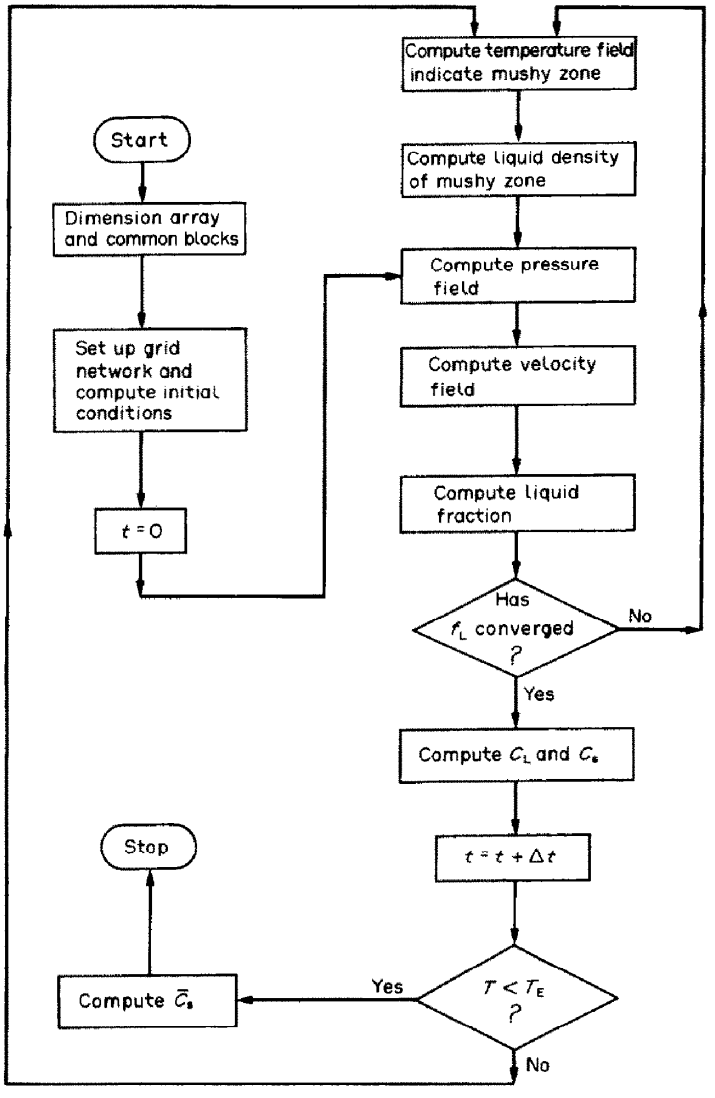

FIG. 2. Flow chart of numerical computation.

other equations, must make these equations nonlinear. If the numerical simulation still adopts the difference method of a linear differential equation, a trial-and-error method is used so that computation accuracy can be improved. A cycle from temperature T to liquid fraction f_L in Fig. 2 performs the method. The process of recalculating T, ρ_L, P, V, and f_L is continued until an insignificant change in f_L is reached (usually after 2–3 calculated sequences in every time interval Δt).

3.2. *Single-valued conditions*

Values for ingot dimension, thermal conditions, and properties of Al–4.5Cu alloy are given in Tables 1 and 2, respectively. Figure 3 shows the Al–Cu binary diagram and liquid density of the alloy vs composition. Boundary conditions for some equations are given as follows.

Table 1. Conditions chosen in test

ingot code	1008	1003
ingot size (m)	$\phi 0.08 \times 0.2$	$\phi 0.08 \times 0.2$
preheating temperature of mould (°C)	550	270
cooling rate (°C s^{-1})†	1.8×10^{-3}	6.0×10^{-1}
solidification time (min)	96	3.4

† The smallest cooling rate in position of half radius 6 cm above the ingot bottom.

3.2.1. *For energy equation.* For simplicity, the boundary conditions of the energy equation are indicated at the surfaces of the ingot. Temperature values of all nodal points on the boundary networks at various times are calculated with interpolation method after temperatures are measured with the thermocouples, installed at the side and bottom of the ingot, as shown in Fig. 4. Therefore, at the side

Table 2. Properties of Al–4.5Cu alloy

liquidus temperature (°C)	645
eutectic temperature (°C)	548
eutectic copos. (wt%)	33Cu
partition ratio	0.172
viscosity (kg m^{-1} s^{-1})	0.003
latent heat of solidification (J kg^{-1})	3.89×10^5
specific heat (J kg^{-1} K^{-1})	1.04×10^3
thermal conductivity (W m^{-1} K^{-1})	87.8†

† This is the value in the liquid–solid phase. It is 132.0 W m^{-1} K^{-1} in the solid phase and 70.0 W m^{-1} K^{-1} in the liquid phase.

$$T = T_B(z, t) \tag{14a}$$

and at the bottom

$$T = T_B(r, t). \tag{14b}$$

The top of the ingot is in direct touch with ambient, so

$$-\lambda \frac{\partial T}{\partial z} = h(T - T_A). \tag{15}$$

At the centreline

$$\frac{\partial T}{\partial r} = 0. \tag{16}$$

3.2.2. *For pressure equation.* Along the liquidus isotherm there are only the atmospheric pressure and the static pressure of bulk metal liquid if the effect of convection in the bulk liquid is left out of consideration, and the pressure, P_L, is calculated using the below equation:

$$P_L = P_a + \rho_{L0} g H(r). \tag{17}$$

At the eutectic isotherm the densities of eutectic–liquid and eutectic–solid, i.e. ρ_{LE} and ρ_{sE}, are not equal so that there must be flow to compensate for the solidification shrinkage of the eutectic. This requirement is

$$\mathbf{V}_P = \frac{\rho_{LE} - \rho_{sE}}{\rho_{LE}} \mathbf{U}_E. \tag{18}$$

In the two-dimensional coordinate, $\mathbf{V}_P = V_{rP}\mathbf{r}_0 + V_{zP}\mathbf{z}_0$ and $\mathbf{U}_E = U_{rE}\mathbf{r}_0 + U_{zE}\mathbf{z}_0$. Combining equations (18) and (7) gives

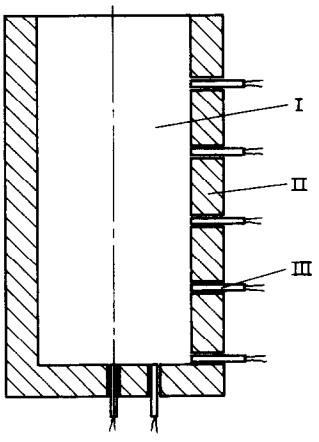

FIG. 4. Position of thermocouple: I, ingot; II, mould; III, thermocouple.

$$\frac{\partial P}{\partial r} = \frac{\mu f_L}{K} \frac{\rho_{sE} - \rho_{LE}}{\rho_{LE}} U_{rE} \tag{19a}$$

$$\frac{\partial P}{\partial z} = \frac{\mu f_L}{K} \frac{\rho_{sE} - \rho_{LE}}{\rho_{LE}} U_{zE} - \rho_L g. \tag{19b}$$

At the centreline

$$\frac{\partial P}{\partial r} = 0. \tag{20}$$

The temperature of the alloy at the ingot–mould interface may be above the eutectic temperature during the initial stage of solidification. This case requires

$$\frac{\partial P}{\partial r} = 0 \qquad \text{at } r = R \tag{21a}$$

$$\frac{\partial P}{\partial z} = -\rho_L g \qquad \text{at } z = 0. \tag{21b}$$

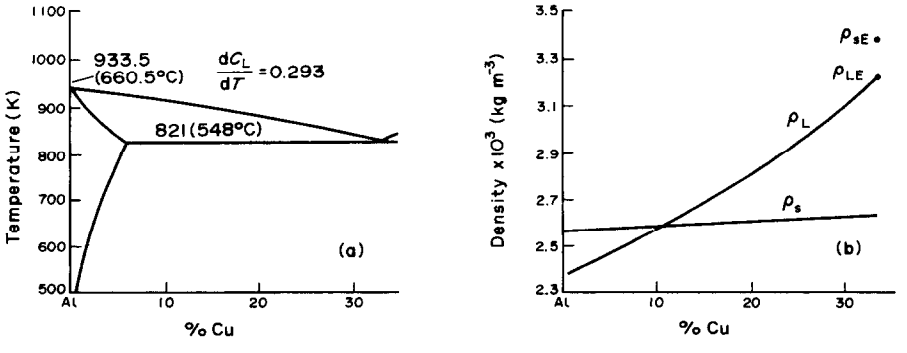

FIG. 3. (a) Binary phase diagram. (b) Densities vs composition for Al–Cu alloy.

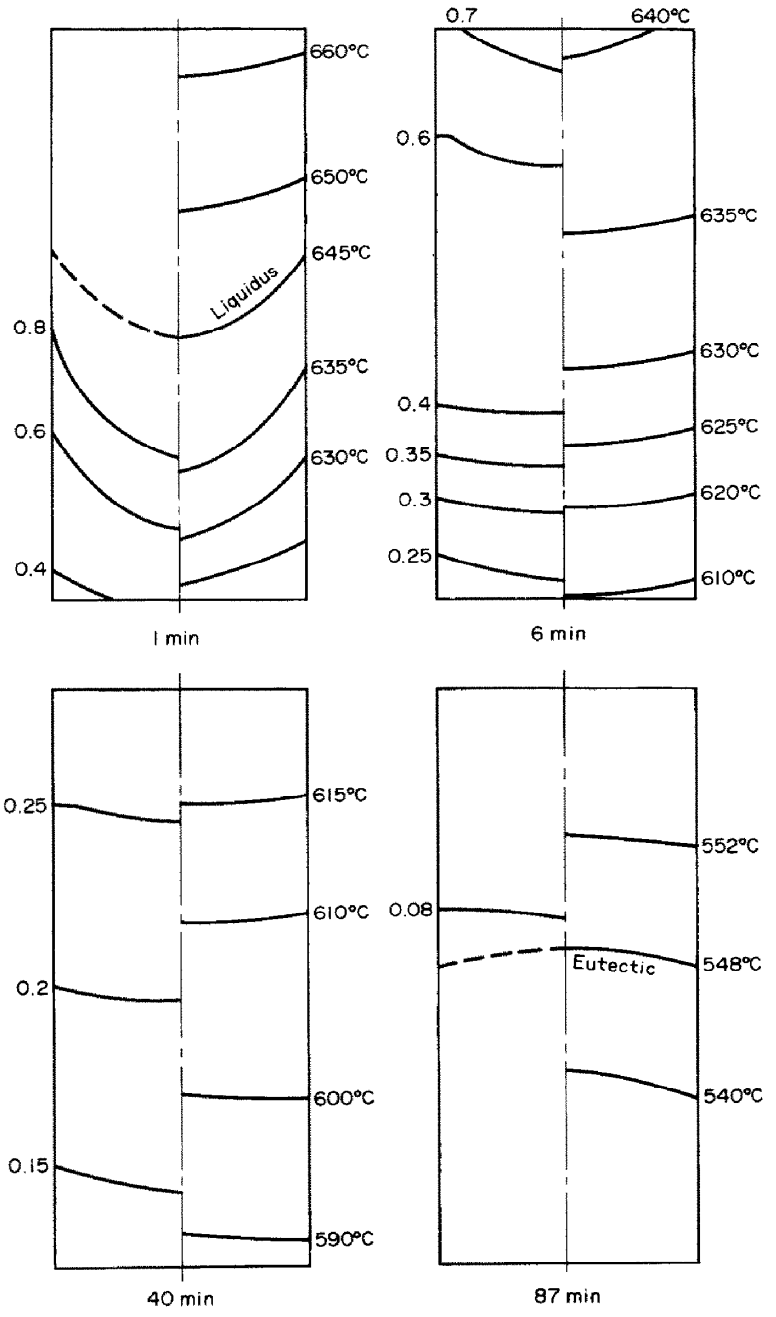

FIG. 5. Calculated isotherm and liquid fraction isoline of ingot No. 1008.

4. RESULTS AND DISCUSSIONS

The right half of each figure in Fig. 5 is the calculated isotherm profile and the left half the calculated isoline profile of the liquid fraction at four different times under the cooling condition of ingot No. 1008 in Table 1. It can be seen by comparison that the isoline of $f_L = 0.35$ always corresponds to the 625°C isotherm, that is, 65% liquid metal has frozen when the temperature falls from liquidus to 625°C. Figure 6 shows the profiles of interdendritic fluid flow in the mushy zone at the same four times as Fig. 5: calculated flow velocity on the left-hand side of each figure and calculated streamline on the right-hand side. The following aspects can be analysed from Figs. 5 and 6.

(1) Back-flow toward the cylindrical axis exists in the radial direction. It can be found by comparing velocity profiles with isotherms at different times that the radial back-flow area which corresponds to the mushy zone above the 625°C isotherm moves toward

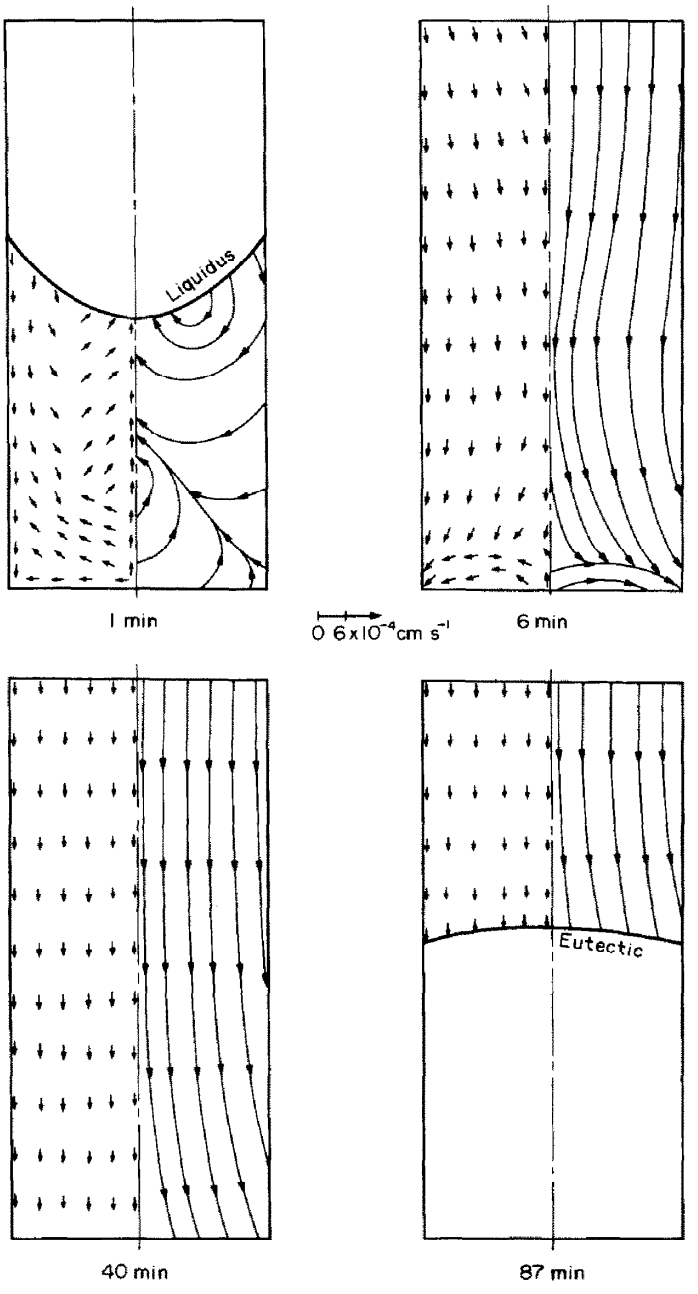

FIG. 6. Calculated velocity profiles in the mushy zone of ingot No. 1008.

the top and the centreline of the ingot with increasing time.

(2) It can be seen from streamline profiles that the back-flow of the whole mushy zone disappears after 40 min when the temperature of the ingot falls below 620°C.

(3) The flow direction in Fig. 6 is similar to that in Fig. 1(a) since $d\rho_L/dT$ of the Al–4.5Cu alloy is less than zero from data of Fig. 3.

(4) The order of magnitude of the interdendritic flow velocity is 10^{-4} cm s^{-1}, and the concrete values of the velocities are in reference to the length of a ray in the velocity profiles of Fig. 6.

(5) Another natural convection exists near the bottom of the ingot besides the main convection near the vertical wall (Fig. 6(a)), but the second-rate convection has become very small after 6 min (Fig. 6(b)). It is considered by preliminary analysis that the second-rate convection is formed due to the large temperature difference above the horizontal bottom in the initial stage of solidification. The second-rate convection has no evident influence on the final com-

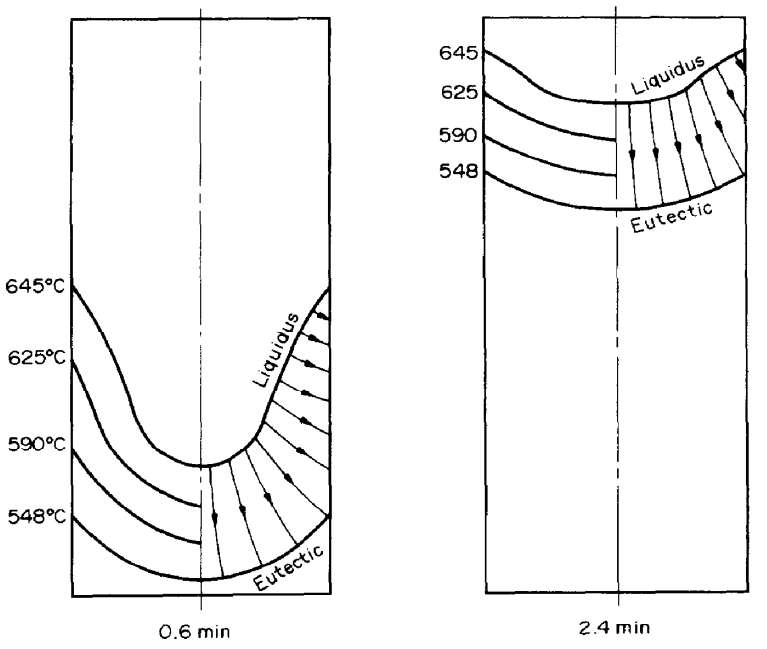

FIG. 7. Isothermal profiles and streamlines of ingot No. 1003 at two times.

position distribution of the ingot since its action is short term.

Figure 7 shows calculated isotherm profiles and streamlines at two different times under the cooling condition of ingot No. 1003 in Table 1. It can be seen by comparison of Fig. 5 with Fig. 7 that the isotherm velocity U changes with different solidifying conditions given in Table 1. The temperature gradient ∇T in the ingot only changes slightly due to great thermal diffusivity of the alloy and release of latent heat during solidification. According to equation (22), U is in direct proportion to the cooling rate ε under conditions of constant ∇T

$$U = -\frac{\varepsilon}{\nabla T}. \tag{22}$$

The smaller the cooling rate, the smaller the isotherm velocity. Therefore, the cooling rate during solidification plays an important role in producing convection in a mushy zone. When isotherms move fast at a large cooling rate such as greater than 10^{-1}°C s^{-1}, the siphonic force due to solidification shrinkage mainly results in the interdendritic flow and gravity acting on a fluid of variable density cannot play an effective role so that natural convection in the mushy zone is not evident. With a decreasing cooling rate, movement of the isotherm is gradually getting slower, and the gravity force can change the flow direction and cause the back-flow due to natural convection. The cooling rate of ingot No. 1008 discussed here is of the order of 10^{-3}°C s^{-1}.

Interdendritic flow due to the siphonic force moves from liquidus to eutectic, as shown with streamline profiles in Fig. 7. The streamlines are almost perpendicular to the isotherms of different times. Any back-flow similar to Fig. 6 is not formed in the two-phase zone, and this indicates that natural convection due to the gravity has little effect on the flow when the cooling rate gets large.

The ratio between interdendritic flow due to gravity and one due to siphonic force varies with cooling rate during solidification, and the flow velocities caused by them can be estimated with the two equations below. For flow velocity due to siphonic force $\mathbf{V}_s$

$$\mathbf{V}_s = \frac{\beta}{1-\beta}\mathbf{U} \tag{23}$$

and for velocity due to gravity V_c [7]

$$V_c = \frac{v f_L^{n-1} \rho_L g \beta_T \Delta T(|1+N|)}{\mu} \tag{24}$$

where the buoyancy ratio $N = \beta_c \Delta C_L / \beta_T \Delta T$ [12].

It is necessary to define a velocity ratio Q

$$Q = \frac{V_c}{|\mathbf{V}_s|}. \tag{25}$$

The dependence of the ratio Q on the cooling rate ε as shown in Fig. 8 is built up on the basis of computation. When ε is greater than a value such as 4.5×10^{-2}°C s^{-1} for the Al–4.5Cu alloy, the value of Q gets smaller and smaller, that is, the flow due to the siphonic force has an effective influence and the one due to gravity has little effect, and vice versa.

5. CONCLUSIONS

(1) The main equations for numerical simulation of convection in a mushy zone based on a model of the

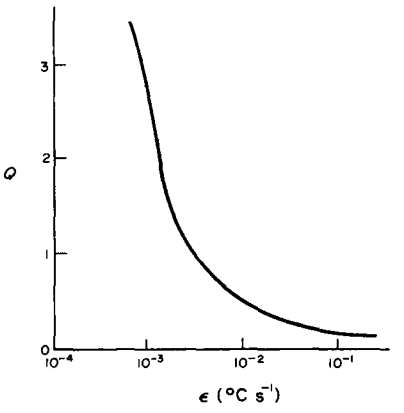

FIG. 8. Dependence of ratio Q on cooling rate ε.

continuum approach to porous medium have been advanced. In order to solve non-linear computation caused by the interaction of unknown variables in the set of equations, the trial-and-error method is used. A cycle from temperature T to liquid fraction f_L in Fig. 2 performs the method. This process of recalculating T, ρ_L, P, $\mathbf{V}$, and f_L is continued until an insignificant change in f_L is reached.

(2) Under the cooling condition of about 10^{-3}°C s^{-1}, the extent and size of radial back-flow due to natural convection in a mushy zone at different times are indicated from calculated velocity profiles. The radial back-flow area exists in the mushy zone above the 625°C isotherm and the back-flow area disappears when the temperature of the whole ingot falls below 625°C.

(3) With increasing cooling rate, interdendritic flow due to siphonic force gets more and more important and one due to gravity more and more secondary. The dependence of the velocity ratio Q defined by equation (25) on the cooling rate expresses the relation mentioned above: the greater the cooling rate, the smaller the ratio Q, and vice versa.

Acknowledgement—The authors especially thank operators of the VAX8300 computer system in No. 618 Research Institute for helping with the numerical computation.

REFERENCES

1. R. Mehrabian, M. Keane and M. C. Flemings, Interdendritic fluid flow and macrosegregation; influence of gravity, *Metall. Trans.* **1,** 1209–1220 (1970).
2. S. D. Ridder, S. Kou and R. Mehrabian, Effect of fluid flow on macrosegregation in axis-symmetric ingots, *Metall. Trans.* **12B,** 435–447 (1981).
3. A. L. Maples and D. R. Poirier, Convection in the two-phase zone of solidifying alloys, *Metall. Trans.* **15B,** 163–172 (1984).
4. W. D. Bennon and F. P. Incropera, Numerical simulation of binary solidification in a vertical channel with thermal and solutal mixed convection, *Int. J. Heat Mass Transfer* **31,** 2147–2160 (1988).
5. Q. Yu and Y. Zhou, Influence of mould rotation on macrosegregation in ingot, *Acta Metall. Sin.* (*Engng Edn*), Series B **2,** 81–86 (1989).
6. J. Bear, *Dynamics of Fluid in Porous Media*, p. 16. American Elsevier, New York (1972).
7. Q. Yu, Research on formation, control, and numerical simulation of channel segregation, Ph.D. Thesis, Northwestern Polytechnical University, Xian, China (1988).
8. M. C. Flemings and G. E. Nereo, Macrosegregation Part 1, *Trans. TMS–AIME* **239,** 1449–1460 (1967).
9. K. Murakami, A. Shiraishi and T. Okamoto, Interdendritic fluid flow normal to primary dendrite-arms in cubic alloys, *Acta Metall.* **31,** 1417–1424 (1983).
10. C. F. Gerald, *Applied Numerical Analysis*, 2nd Edn. Addison-Wesley, California (1978).
11. D. N. Petrakis, M. C. Flemings and D. R. Poirier, Some effects of forced convection on macrosegregation. In *Modeling of Casting and Welding Processing*, pp. 285–312. TMS–AIME, Warrendale, Pennsylvania (1981).
12. A. Bejan and K. R. Khair, Heat and mass transfer by natural convection in a porous medium, *Int. J. Heat Mass Transfer* **28,** 909–918 (1985).

APPENDIX: DERIVATION OF EQUATION (8)

Assuming ρ_s = constant, combining equations (2) and (3) provides

$$-\nabla\cdot(\rho_L f_L \mathbf{V}) = (\rho_L-\rho_s)\frac{\partial f_L}{\partial t} + f_L\frac{\partial \rho_L}{\partial t}. \quad \text{(A1)}$$

Substituting equation (6) for equation (A1) gives

$$\rho_L\nabla\cdot(f_L\mathbf{V}) + f_L\mathbf{V}\cdot\nabla\rho_L = (\rho_L-\rho_S) \times\left[\frac{\rho_L}{\rho_s(1-k)}\left(1+\frac{\mathbf{V}\cdot\nabla T}{\varepsilon}\right)\frac{f_L}{C_L}\frac{\partial C_L}{\partial t}\right] - f_L\frac{\partial \rho_L}{\partial t}. \quad \text{(A2)}$$

From the chain rule

$$\nabla\rho_L = \frac{1}{\varepsilon}\frac{\partial \rho_L}{\partial t}\nabla T. \quad \text{(A3)}$$

Combining equations (A3) and (A2) provides

$$\rho_L\nabla\cdot(f_L\mathbf{V}) + \left(f_L\frac{\nabla T}{\varepsilon}\frac{\partial \rho_L}{\partial t} - a\frac{f_L}{C_L}\frac{\nabla T}{\varepsilon}\frac{\partial C_L}{\partial t}\right)\cdot\mathbf{V} = a\frac{f_L}{C_L}\frac{\partial C_L}{\partial t} - f_L\frac{\partial \rho_L}{\partial t} \quad \text{(A4)}$$

where $a = \rho_L(\rho_L-\rho_s)/\rho_s(1-k)$. Assuming

$$b = \frac{f_L}{\rho_L}\frac{dC_L}{dT}\left(\frac{\partial \rho_L}{\partial C_L} - \frac{a}{C_L}\right)$$

equation (A4) can be simplified as

$$\nabla\cdot(f_L\mathbf{V}) + b\nabla T\cdot\mathbf{V} + b\varepsilon = 0. \quad \text{(A5)}$$

Substituting equation (7) for equation (A5) gives

$$\nabla^2 P + \left[\frac{\mu}{K}\nabla\left(\frac{K}{\mu}\right) + b_1\frac{\nabla T}{\rho_L}\right]\cdot\nabla P + \frac{\mu}{K}\nabla\cdot\left(\frac{K}{\mu}\rho_L\mathbf{g}\right) + b_1\nabla T\cdot\mathbf{g} - b_1\frac{\mu f_L}{K\rho_L}\varepsilon = 0 \quad \text{(A6)}$$

where $b_1 = b(\rho_L/f_L)$. In axisymmetric coordinates there are

$$\nabla P = \frac{\partial P}{\partial r}\mathbf{r}_0 + \frac{\partial P}{\partial z}\mathbf{z}_0 \quad \text{(A7a)}$$

$$\nabla^2 P = \frac{\partial^2 P}{\partial r^2} + \frac{1}{r}\frac{\partial P}{\partial r} + \frac{\partial^2 P}{\partial z^2} \quad \text{(A7b)}$$

$$\nabla T = \frac{\partial T}{\partial r}\mathbf{r}_0 + \frac{\partial T}{\partial z}\mathbf{z}_0. \quad \text{(A7c)}$$

Assuming $K = vf_L^2$ and the viscosity of the alloy is taken as constant [1], we have

$$\frac{\mu}{K}\nabla\left(\frac{K}{\mu}\right) = \frac{2}{f_L}\left(\frac{\partial f_L}{\partial r}\mathbf{r}_0 + \frac{\partial f_L}{\partial z}\mathbf{z}_0\right) \tag{A8a}$$

$$\frac{\mu}{K}\nabla\cdot\left(\frac{K}{\mu}\rho_L\mathbf{g}\right) = g\frac{\partial \rho_L}{\partial z} + \frac{2g\rho_L}{f_L}\frac{\partial f_L}{\partial z}. \tag{A8b}$$

After substituting equations (A7) and (A8) for equation (A6), an expression for the pressure distribution in the mushy zone during solidification, i.e. equation (8) can be obtained.

SIMULATION NUMERIQUE DE LA CONVECTION DANS LA DEUX-PHASE ZONE D'ALLIAGE BINAIRE

Résumé—L'équation fondamentalle pour simulation numérique de convection à la deux-phase zone se base sur un modèle de médium continu à l'approche du modèle poreux. On prend une méthode d'éssai pour résoudre un comptage non-linéaire causé par une intération de variables non-savoir dans les équations. Les limite et dimension de la fluide interdendritique dans des temps différents sont indiquées sur des profils de vitesses calculées. On voit que la retour-fluide radialle correspond à la zone de solidification au dessus de l'isotherme de 625°C sous les conditions de la petite vitesse de refroidissement. En croissant la vitesse de refroidissement, de plus en plus important devient le fluide du à la force du siphon.

NUMERISCHE SIMULATION DER KONVEKTION IN DER ZWEI PHASEN-ZONE VON DEN BINÄREN LEGIERUNGEN

Zusammenfassung—Die Grundgleichungen für numerische Simulation der Konvektion in der zwei Phasen-Zone gründet auf dem Modell vom Kontinuum des porösen Mediums. Um die nichtlineare Berechnung zu lösen, die durch die sich gegenseitig beeinflussenden unbekannten Variablen in den verschiedenen Gleichungen verursacht wird, wird die Versuchsmethode angewandt. Der Bereich und die Grösse der interdendritischen Strömung, die durch die natürlichen Konvektion in den verschiedenen Zeitpunkten veranlasst wird, können durch die berechnete Geschwimdig-keitsdiagramme angezeigt werden. Daraus ist zu ersehen, dass die radiale Rückströmungszone unter der Bedingung der kleinen Kühlgeschwindigkeit mit der Schmelzzone über der 625°C-Isotherme korrespondiert. Mit der Steigerung der Kühlgeschwindigkeit wird die von der siphonik bewirkte Strömung immer wichtiger.

ЧИСЛЕННОЕ МОДЕЛИРОВАНИЕ КОНВЕКЦИИ В ДВУХФАЗНОЙ ЗОНЕ БИНАРНОГО СПЛАВА

Аннотация—Получены основные уравнения для численного моделирования конвекции в двухфазной зоне на основе рассмотрения пористой среды как сплошной. Для решения нелинейной задачи, связанной с наличием неизвестных переменных в уравнениях, используется метод проб и ошибок. Размер и протяженность междендритного потока в различные моменты времени определяются по рассчитанным профилям скоростей. Показано, что радиальная область обратного течения, обусловленная естественной конвекцией, соответствует пористой зоне над изотермой 625 °C в условиях низкой скорости охлаждения. С ростом скорости охлаждения вызванное сифонной силой течение приобретает все большее значение.